ISSN 1070-3284, Russian Journal of Coordination Chemistry, 2021, Vol. 47, No. 12, pp. 881–890. © Pleiades Publishing, Ltd., 2021.

Binuclear Complexes of Cu(II) and Mg(II) with 2-Furancarboxylic Acid: Synthesis, Structure, EPR Spectroscopy, and Results of In Vitro Biological Activity against *Mycolicibacterium smegmatis* and *SCOV3*

I. A. Lutsenko[a, *], M. E. Nikiforova[a], K. A. Koshenskova[a, b], M. A. Kiskin[a], Yu. V. Nelyubina[c], P. V. Primakov[c], M. V. Fedin[d], O. B. Becker[e], V. O. Shender[f], I. K. Malyants[b, f], and I. L. Eremenko[a, c]

[a] *Kurnakov Institute of General and Inorganic Chemistry, Russian Academy of Sciences, Moscow, Russia*

[b] *Mendeleev University of Chemical Technology of Russia, Moscow, Russia*

[c] *Nesmeyanov Institute of Organoelement Compounds, Russian Academy of Sciences, Moscow, Russia*

[d] *International Tomography Center, Siberian Branch, Russian Academy of Sciences, Novosibirsk, Russia*

[e] *Vavilov Institute of General Genetics, Russian Academy of Sciences, Moscow, Russia*

[f] *Federal Scientific and Clinical Center of Physicochemical Medicine, Federal Medical and Biological Agency, Moscow, Russia*

**e-mail: irinalu05@rambler.ru*

Received June 8, 2021; revised July 12, 2021; accepted July 13, 2021

Abstract—Using the reactions of copper(II) acetate magnesium(II) oxide with 2-furancarboxylic acid (HFur), compounds with chemical compositions $[Cu_2(Fur)_4(MeCN)_2]$ (**I**) and $[Mg_2(Fur)_4(H_2O)_5]\cdot MeCN\cdot H_2O$ (**II**) are synthesized. According to the X-ray diffraction data (CIF files CCDC nos. 2085817 (**I**) and 2085818 (**II**)), both complexes have a binuclear structure. The metal core of **I** correspond to the tetracarboxylate bridged $\{Cu_2(\mu\text{-}Fur)_4\}$ complex, the coordination number of the copper atom in which is 5 ($CuNO_4$); in **II**, the metal atoms are linked by two carboxylate groups and a water molecule, and the coordination environment of the metal centers is completed to the polyhedron (MgO_6) by oxygen atoms of the Fur^- anions and water molecules. According to EPR spectroscopy data, exchange-coupled copper(II) dimers with a substantial zero-field splitting are observed in **I**. For **I** and **II**, antibacterial activity against the nonpathogenic strain of *M. smegmatis*, and cytotoxicity against human ovarian adenocarcinoma cells *SCOV3* and normal human fibroblast cells of the *HDF* line have been determined.

Keywords: copper(II), magnesium, 2-furancarboxylic acid, crystal structure, EPR spectroscopy, biological activity

DOI: 10.1134/S1070328421350013

INTRODUCTION

The development of targeted medicinal chemistry is associated with the search for biologically active molecules capable of simultaneously affecting several biotargets (cell wall components, DNA metabolism, mechanisms for blocking transcription/translation processes, etc.) [1–3]. These kinds of molecules can include coordination compounds of a certain chemical composition and structure. Currently, the use of complexes with essential (vital) metals is considered among the strategies for increasing antimicrobial activity, for example, against sensitive multiresistant strains of the tuberculosis mycobacterium (TMB), as well as TMB in the dormant (sleeping) state [4–7].

Being a part of numerous enzymes in living organisms, copper is among the promising biocomplex formation agents and performs a wide variety of functions (for example, the redox function as a component of the enzymes of the respiratory chain) [8–12]. A recent study on the chemotherapeutic drug elesklomol (effective against MBT H37Rv with a minimum inhibitory concentration (MIC) of 4 mg/L) by Ngwane has demonstrated a more than 65-fold increase in the efficiency of complex formation with copper(II) [9, 13]. Magnesium is also among the important biometals, which is involved in a cascade of energy metabolism reactions and takes part in the conduction of neural impulses, the contraction of muscle fibers, the production of nucleic acids, etc. [14, 15]. However, complex formation with Mg^{2+} ions often exhibits completely different binding schemes than the corresponding compounds of IIA-group metals [16–26]. This effect is primarily caused by differences in the charge-to-ionic radius ratio (0.801 for Mg^{2+}, 0.987 for

Ca^{2+}, 1.076 for Sr^{2+}, and 1.118 for Ba^{2+} [27]). For example, magnesium often tends to be surrounded by water molecules rather than carboxylate anions when interacting with carboxylate anions (this fact was additionally confirmed by quantum chemical calculations [28]). Our earlier studies [29–34] on the in vitro biological activity of furoate complexes of Fe(III), Co(II), Ni(II), Cu(II), and Zn(II) with various N,O-donor ligands showed their effectiveness against nonpathogenic mycobacterial strain *Mycolicibacterium smegmatis*. In this connection, the aims of this study were developing a procedure for the synthesis of Cu(II) and Mg(II) complexes with 2-furancarboxylic acid anions (HFur), i.e., $[Cu_2(Fur)_4(MeCN)_2]$ (**I**) and $[Mg_2(Fur)_4(H_2O)_5]\cdot MeCN\cdot H_2O$ (**II**), elucidating the structure of the obtained compounds and the nature of electronic interactions from the EPR spectroscopy data for **I**, and determining the in vitro biological activity against model nonpathogenic strain *Mycolicibacterium smegmatis* and human ovarian adenocarcinoma cells (*SCOV3*) for complexes **I** and **II**.

EXPERIMENTAL

The complexes were synthesized in air using distilled water and the following solvents without additional purification: acetonitrile (special purity grade, Khimmed) and ethanol (96%). The following commercially available reagents were used in the syntheses: 2-furancarboxylic acid (98%, Acros), copper(II) acetate monohydrate (95%, Acros), and MgO (97%, Acros).

The elemental analyses were performed on a Carlo Erba EA 1108 automatic C,H,N analyzer. The IR spectra of the compound were recorded on a Perkin-Elmer Spectrum 65 FTIR spectrophotometer using the ATR method in the frequency range of 400–4000 cm^{-1}. The Q-band (34 GHz) EPR spectra were recorded on a Bruker Elexsys E580 commercial spectrometer in a steady-state mode. An Oxford Instruments system was used for the temperature control ($T = 4$–300 K). All calculations were performed using the EasySpin software package for the Matlab environment [35].

The biological activities of **I** and **II** were determined in the *M. smegmatis* mc^2 155 test system by the paper disk method. The sizes of the growth inhibition zone of the lawn strain seeded in an agar medium around paper disks containing the substance in various concentrations were measured. The bacteria washed off from Petri dishes with an M-290 Trypton soybean agar medium (Himedia) were grown overnight in a Lemco-TW liquid medium containing 5 g L^{-1} of Lab Lemco' Powder (Oxoid), 5 g L^{-1} of Peptone special (Oxoid), 5 g L^{-1} of NaCl, and Tween-80 at 37°C until the average logarithmic growth phase and were mixed with an M-290 molten agar medium in a ratio of 1 : 9 : 10 (bacterial culture : Lemco-TW : M-290) upon reaching an optical density of OD600 = 1.5. The culture was incubated for 24 h at 37°C. The concentration of the substance at which the growth inhibition zone has a minimum size was considered to be MIC. The *M. smegmatis* test system exhibits a higher degree of resistance to antibiotics and anti-tuberculosis agents against *M. tuberculosis*; therefore, a substance concentration of <100 μg/disc was chosen as a selection criterion. The test method involves quantifying the diameter of the growth inhibition zone of the *M. smegmatis* culture grown in an agar lawn around paper disks soaked in test compounds. The test compounds were applied to discs in different concentrations and the halo diameter (growth inhibition zone) was measured.

The cytotoxic effect of various concentrations of complexes **I** and **II** on human ovarian adenocarcinoma cells *SCOV3* and human dermal fibroblasts (*HDF*) was measured using the MTT test. This test is based on measuring the activity of the mitochondrial enzyme succinate dehydrogenase and is widely used to assess the anticancer activity of potential drugs in vitro. Using to the MTT test data, the half-maximum inhibition concentration (IC50) was calculated for both substances. Cells of *SCOV3* were obtained from the ATCC collection, and the primary *HDF* culture was obtained from a healthy donor. The *SCOV3* and *HDF* cells were cultivated in a DMEM medium (10% FBS, 2 mM glutamine, and 1% genmaticin). The cells were cultivated in plastic flasks under sterile conditions and were incubated at 37°C in the presence of 5% CO_2.

The stock solutions (50 mM) of compounds **I** and **II** were prepared in DMSO; before adding to the cells, they were diluted to the required concentrations in a culture medium, and *SCOV*3 and *HDF* were seeded in the wells of 96-well plates in the amount of 4×10^3 cells per well and 3.5×10^3 cells per well, respectively. The cells were allowed to fix for 14 h, after which different concentrations of the test compounds or DMSO (as a control sample) were injected in triplicate by the titration method. The final volume of the medium in the wells was 100 μL. At the end of the period of 48 h after the addition of samples, the cell viability was measured using the MTT reagent (Sigma). The 10 μL volumes of an MTT working solution (7 mg/mL) were added to each well with cells (100 μL of a medium) and the wells were incubated for 3 h, after which the medium was replaced with a DMSO solution. Using a tablet spectrophotometer (TECAN Infinite M Plex), the absorbance of each well was determined at 570 nm with subsequent subtraction of the background absorbance. The concentration value and the IC50 inhibition dose were determined from the dose–response curves.

Synthesis of $[Cu_2(Fur)_4(MeCN)_2]$ (I). Weighed portions of $Cu(OAc)_2\cdot H_2O$ (0.182 g, 1 mmol) and HFur (0.224 g, 2 mmol) were dissolved in 40 mL of MeCN. The resulting reaction mixture was held at

70°C for 3 h. The resulting blue-green solution was filtered and concentrated to a volume of 20 mL. Green crystals formed after one day, which were separated from the mother liquor by decantation, washed with MeCN, and dried in air. Yield of **I** 0.25 g (76%).

For $C_{24}H_{18}O_{12}N_2Cu_2$ (**I**)

Anal. calcd., %	C, 44.11	H, 2.88	N, 4.29
Found, %	C, 44.23	H, 3.06	N, 4.41

IR (ν, cm–1): 3360 mw, 3134 w, 3120 w, 3079 w, 3060 w, 3023 vw, 1695 mw, 1601 m, 1568 vw, 1495 m, 1481 s, 1474 vs, 1447 w, 1385 vs, 1370 vs, 1356 vs, 1322 vw, 1286 w, 1258 w, 1257 w, 1225 m, 1172 m, 1187 vs, 1137 m, 1126 w, 1075 m, 1056 m, 1032 vw, 1019 vs, 1007 vs, 928 s, 896 vw, 883 s, 853 w, 812 m, 782 s, 766 vs, 731 m, 663 w, 650 w, 598 mw, 547 mw, 468 s.

Synthesis of $[Mg_2(Fur)_4(H_2O)_5]\cdot MeCN\cdot H_2O$ (II). Ethanol (25 mL) was added to weighed portions of MgO (0.100 g, 2.48 mmol) and HFur (0.556 g, 4.96 mmol), and the mixture was stirred at 70°C until the components were completely dissolved. The resulting clear solution was evaporated to dryness, and 10 mL of a mixture of solvents MeCN : EtOH (1 : 1) was added to the residue. The reaction mixture was held at room temperature while the solvent was slowly evaporating. Colorless rectangular crystals that were precipitated after two weeks were separated from the solution by decantation and dried in air. Yield of **II** 0.65 g (81% based on the initial amount of MgO).

For $C_{22}H_{27}O_{18}NMg_2$

Anal. calcd., %	C, 41.16	H, 4.33	N, 2.18
Found, %	C, 42.06	H, 4.24	N, 2.22

IR (ν, cm–1): 3522 m, 3358 mm, 3145 w, 3131 vw, 1615 s, 1580 s, 1479 vs, 1415 s, 1397 vs, 1368 vs, 1228 m, 1195 s, 1144 m, 1127 m, 1079 m, 1015 s, 932 m, 884 m, 844 w, 784 vs, 752 vs, 613 w, 596 m, 549 vs, 481 m.

X-ray diffraction structural analysis. The X-ray diffraction studies of complexes **I** and **II** were performed on a Bruker Apex II DUO diffractometer (CCD detector, MoK_α radiation, λ = 0.71073 Å, graphite monochromator) at 120 K. The structures were deciphered using the ShelXT software package [36] and refined by the full-matrix least squares method using the Olex2 software package [37] in the anisotropic approximation for non-hydrogen atoms. The hydrogen atoms of the water molecule are localized on the basis of difference Fourier maps, and the positions of the remaining hydrogen atoms are calculated geometrically. All the positions are refined in the isotropic approximation according to the rider model. The diffuse contribution of disordered solvent molecules was described using the Bypass option (a.k.a. squeeze) of the software package [37]. The main crystallographic data and refinement parameters are given in Table 1.

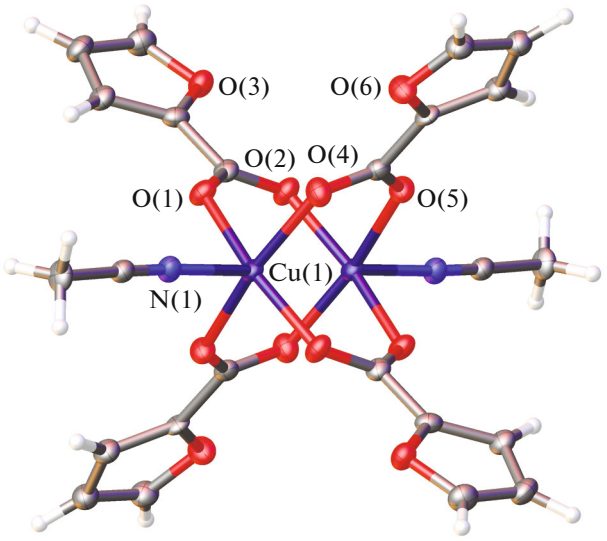

Fig. 1. General view of complex **I**. Hydrogen atoms are not shown for clarity, non-hydrogen atoms are shown as thermal vibration ellipsoids (p = 50%), and the numbering is given only for heteroatoms of the independent part of the unit cell.

The complete set of X-ray structural parameters has been deposited at the Cambridge Crystallographic Data Center (CCDC nos. 2085817 (**I**) and 2085818 (**II**); deposit@ccdc.cam.uk).

RESULTS AND DISCUSSION

According to the results of X-ray diffraction studies, complex **I** crystallizes in triclinic space group $P\bar{1}$ in the form of a solvate with acetonitrile. The structure of the molecule of complex **I**, which occupies a particular position in the crystal at the center of inversion located between two copper(II) ions, corresponds to the Chinese lantern model (Fig. 1, Table 2). The coordination environment of copper(II) ions is formed by four oxygen atoms that belong to four anions of 2-furancarboxylic acid and a nitrogen atom of the coordinated acetonitrile molecule at the vertices of a square pyramid. This type of tetracarboxylate linked motif is quite typical for copper and zinc complexes [29, 38, 39]. In the absence of suitable donors for hydrogen bonding, the molecules of complex **I** are linked by many weak interactions—primarily, by C–H...O and C–H...N contacts—with the formation of a three-dimensional framework (Fig. 2).

In complex **II** (Fig. 3, Table 2), two symmetrically independent magnesium(II) ions are linked by two μ-bridging Fur^- anions (Mg–O 2.013(4)–2.100(4) Å) and the oxygen atom of the water molecule (Mg–O 2.080(4) and 2.131(4) Å). The coordination environment of Mg(2) is completed to a tetragonal bipyramide

Table 1. Crystallographic parameters and details of the refinement of structures **I** and **II**

Parameter	Value	
	I	**II**
Molecular formula	$C_{24}H_{18}Cu_2N_2O_{12}$	$C_{22}H_{27}Mg_2NO_{18}$
M	653.48	642.066
T, K	120	
Crystal system	Triclinic	
Space group	$P\bar{1}$	
Crystal dimensionsions, mm; color	0.2 × 0.1 × 0.1; turquoise-colored	0.3 × 0.2 × 0.1; colorless
a, Å	7.164(3)	10.617(3)
b, Å	9.317(4)	10.990(3)
c, Å	9.953(4)	12.899(3)
α, deg	79.997(8)	102.611(5)
β, deg	71.207(8)	98.929(5)
γ, deg	79.219(9)	91.876(5)
V, Å^3	613.2(4)	1447.4(6)
Z	1	2
ρ(calculated), g/cm^3	1.770	1.473
μ, mm^{-1}	1.806	0.166
F(000)	330	668
Data acquisition region with respect to θ, deg	2.178–25.999	1.64–26.00
Reflection index ranges	$-8 \le h \le 8$, $-11 \le k \le 11$, $-12 \le l \le 12$	$-15 \le h \le 15$, $-15 \le k \le 15$, $-18 \le l \le 18$
Number of measured reflections	5962	19661
Number of independent reflections (R_{int})	2409 (0.0709)	5512 (0.0644)
Number of reflections with $I > 2\sigma(I)$	1890	4082
Number of refinement variables	182	430
GOOF	1.024	1.064
R-factors over $F^2 > 2\sigma(F^2)$	$R_1 = 0.0604$, $wR_2 = 0.1517$	$R_1 = 0.0906$, $wR_2 = 0.2365$
R-factors over all reflections	$R_1 = 0.0785$, $wR_2 = 0.1625$	$R_1 = 0.1153$, $wR_2 = 0.2534$
Residual electron density (min/max), e/Å^3	−1.611/1.709	−0.6140/1.1190

Table 2. Principal bond lengths for **I** and **II**

Bond	*d*, Å
I	
Cu(1)–O(1)	1.971(3)
Cu(1)–O(5)	1.977(4)
Cu(1)–O(2)	1.988(4)
Cu(1)–O(4)	1.979(4)
Cu(1)–N(1)	2.174(4)
II	
Mg(1)–O(1)	2.028(4)
Mg(1)–O(4)	2.100(4)
Mg(1)–O(7)	2.078(4)
Mg(1)–O(10)	2.108(4)
Mg(1)–O(13)	2.131(4)
Mg(1)–O(17)	2.042(3)
Mg(2)–O(2)	2.077(4)
Mg(2)–O(5)	2.013(4)
Mg(2)–O(13)	2.080(4)
Mg(2)–O(14)	2.059(4)
Mg(2)–O(15)	2.108(4)
Mg(2)–O(16)	2.080(4)

by binding to O atoms of three terminal water molecules (Mg–O 2.059(4)–2.108(4) Å), and the coordination environment of the Mg(1) ion is completed to a tetragonal bipyramide by binding to O atoms of a water molecule (Mg–O 2.042(3) Å) and two additional carboxylate anions (Mg–O 2.078(4) and 2.108(4) Å) as monodentate ligands. Uncoordinated O atoms of monodentate Fur^- anions are involved in the formation of intramolecular hydrogen bonds with two hydrogen atoms of the bridging water molecule (O...O 2.535(5)–2.682(5) Å, OHO angle 144°–157°) (Fig. 3). The structure of complex **II** is similar to the structure of well-known complex $[Mg_2(Fur)_4(H_2O)_5]\cdot H_2O$ [40]. The only difference consists in the presence of an additional solvate molecule of acetonitrile. In the crystal of **II**, the molecules of the complex are coupled into centrosymmetric dimers by hydrogen bonds between the H atoms of the terminal water molecule coordinated to the Mg(1) ion and two oxygen atoms of the Fur^- anions coordinated to the analogous magnesium ion (O...O 2.804(5) and 2.826(6) Å, OHO angles 144° and 146°, respectively) (Fig. 4, Table 3). Three more water molecules in the role of terminal ligands for the Mg(2) ion form intermolecular hydrogen bonds with the oxygen atoms of the carboxylate groups of the corresponding anions (O...O 2.749(5)–

Table 3. Geometric parameters of hydrogen bonds in crystal **II***

D–H···A	Distance, Å			D–H···A angle, degree
	D–H	H···A	D···A	
O(13)–H(13A)...O(8A)	0.94	1.72	2.54(3)	144
O(13)–H(13A)...O(8)	0.94	1.65	2.535(5)	157
O(13)–H(13B)...O(11)	0.86	1.87	2.682(5)	157
O(17)–H(17A)...O(4)$^{\#1}$	0.87	2.05	2.804(5)	145
O(17)–H(17B)...O(10)$^{\#1}$	0.87	2.07	2.825(5)	146
O(16)–H(16A)...O(2)$^{\#2}$	0.83	1.99	2.802(5)	167
O(16)–H(16B)...N(1S)$^{\#3}$	0.96	1.89	2.811(8)	160
O(14)–H(14A)...O(16)$^{\#2}$	0.94	2.47	2.983(5)	115
O(14)–H(14A)...O(12)$^{\#4}$	0.94	2.31	2.864(5)	117
O(14)–H(14B)...O(11)$^{\#4}$	0.94	1.92	2.749(5)	145
O(18)–H(18A)...O(8A)$^{\#4}$	0.95	1.75	2.58(3)	143
O(18)–H(18A)...O(8)$^{\#4}$	0.95	1.79	2.723(7)	169
O(18)–H(18B)...O(11)	0.95	2.43	3.139(7)	131
O(15)–H(15A)...O(11)$^{\#4}$	0.94	2.4	3.132(6)	135
O(15)–H(15B)...O(18)	0.94	1.91	2.707(7)	142

* Symmetry codes: $^{\#1}$ $1-x, 1-y, 2-z$; $^{\#2}$ $-x, 1-y, 1-z$; $^{\#3}$ $-x, -y, 1-z$; $^{\#4}$ $1-x, 1-y, 1-z$.

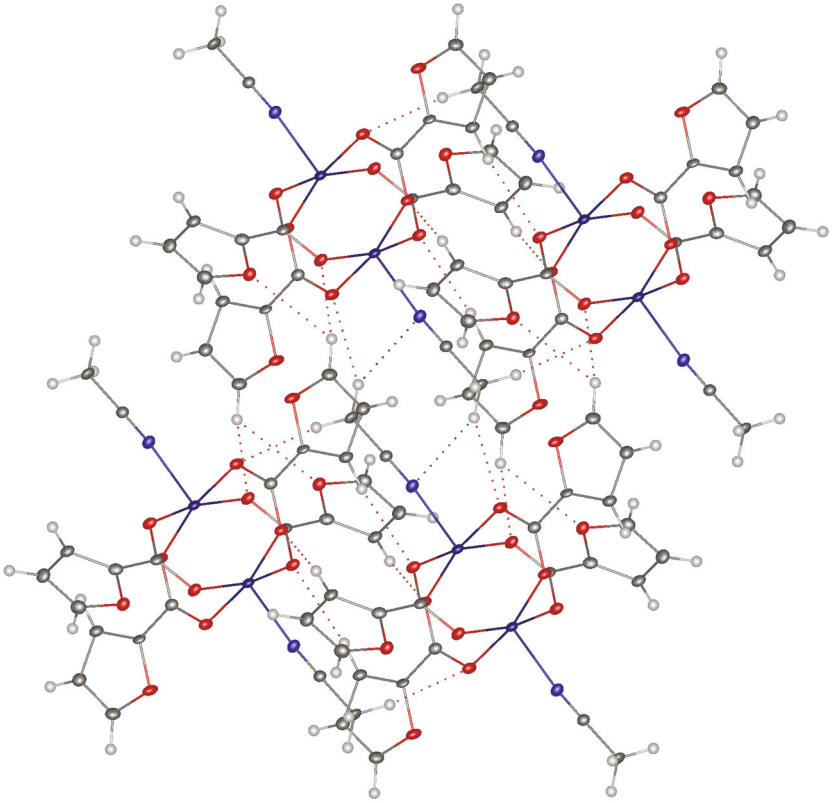

Fig. 2. Fragment of the crystal packing of complex **I**. Dotted lines show the C–H...O and C–H...N contacts.

3.132(6) Å, OHO angle 135°–167°) and O atoms in the heterocycles (O...O 2.864(5) Å, OHO angle 117°). Hydrogen bonds with solvate molecules of water (O...O 2.707(7) Å, OHO angle 142°) and acetonitrile (O...N 2.810(9) Å, OHN angle 160°) complete the formation of a three-dimensional hydrogen-bonded framework.

For complex **I**, steady-state EPR spectra were recorded in the Q-band region at 293 and 150 K (Fig. 5). The spectra are classic patterns of exchange-coupled copper dimers with a substantial zero-field (ZF) splitting and correspond to a thermally populated triplet state. The spectrum intensity noticeably decreases with a decrease in the temperature from 293 (Fig. 5a) to 150 K (Fig. 5b), which points to a strong intramolecular antiferromagnetic exchange interaction with a parameter of about 100–200 cm^{-1}. A small additional peak near 1150 mT—which is well defined at 293 K and weakly visible at 150 K—is a manifestation of weaker interdimer exchange interactions that lead to exchange collapse of some orientations in the crystal [41]. The spectra can be well processed using the following set of parameters: g = [2.06 2.06 2.38], D = 384 mT, $E \sim 0$, and A = [0 0 210] MHz, where D and E are the scalar parameters of the ZF splitting.

The antibacterial activity of compounds **I** and **II** was determined with respect to the nonpathogenic *M. smegmatis* strain. All obtained results on the in vitro biological activity of the studied compounds were compared with the activity of isoniazid (INH) and rifampicinum (Rif) under the same experimental conditions. The substances were applied to the discs in different concentrations. The results of antibacterial activity in test system *M. smegmatis* mc^2 155 and its change over time for compounds **I** and **II** are shown in Table 4. As can be seen from the data provided in Table 4, compound **I** exhibits the biological activity approximately comparable to the activity of individual HFur. However, in comparison with the previously investigated copper(II) complexes—for example, $[Cu(Fur)_2(Bipy)(H_2O)]$ and $[Cu(Fur)_2(Phen)]$, in which the appearance of additional Bipy/Phen ligands (in addition to 2-furancarboxylic acid) markedly enhances the bioactivity of compounds [29, 31]—the activity of **I** is substantially lower. In contrast to **I**, complex **II** barely exhibits biological activity (Table 4). Its MIC value is among the lowest ones in the investigated series of furancarboxylate complexes of Fe(III), Co(II), Cu(II), and Zn(II) (Table 4) [29–34]. Thus, the following dependence of the sensitivity of the mycobacterial wall to cations can be drawn:

$$\underset{\text{Biological activity}}{\text{Ni Mg Co Zn Fe Cu} \longrightarrow}$$

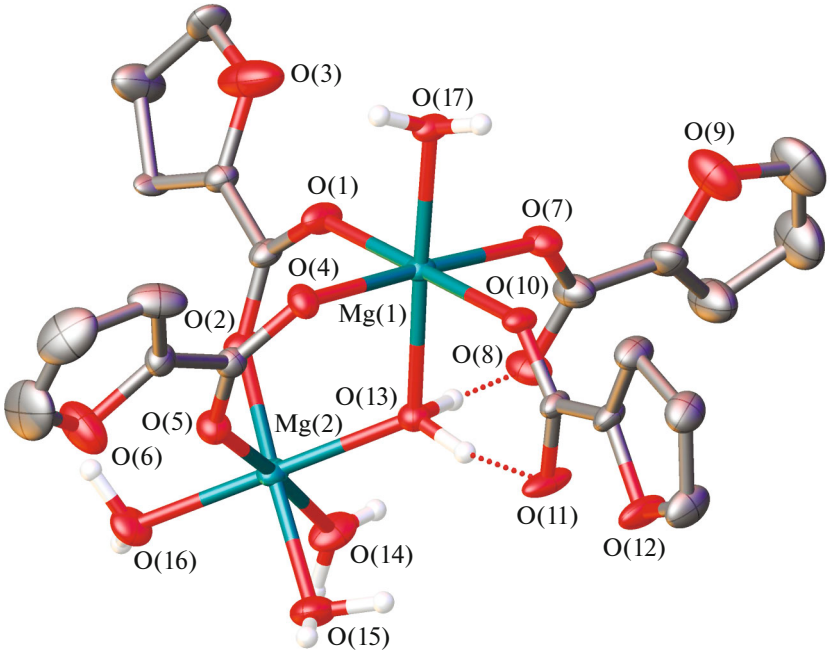

Fig. 3. General view of complex **II**. Hereinafter, hydrogen atoms (with the exception of those belonging to water molecules) and minor components of disordered 2-furancarboxylic acid anions are not shown, non-hydrogen atoms are shown as thermal vibration ellipsoids ($p = 30\%$), and hydrogen bonds are shown by dashed lines.

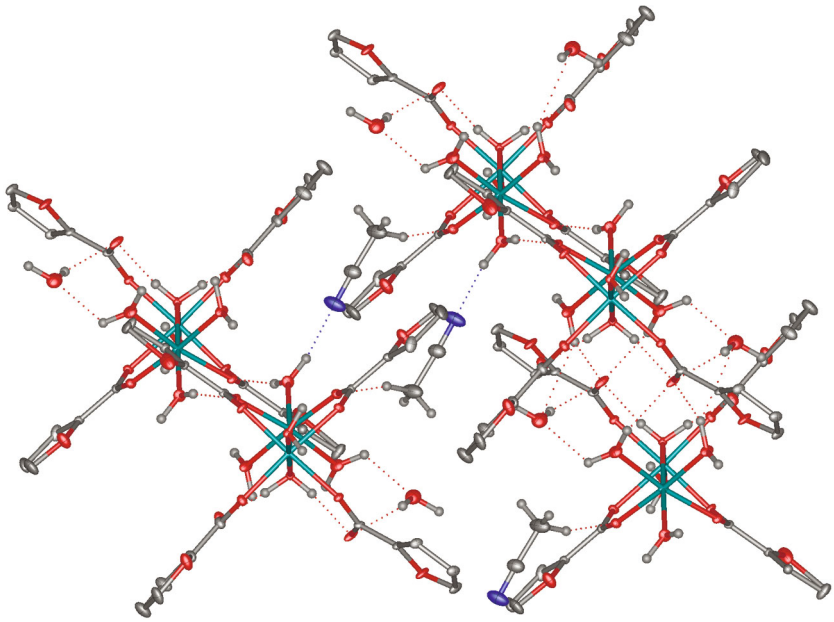

Fig. 4. Fragment of the crystal packing illustrating the formation of hydrogen bonds in crystal **II**.

For complexes **I** and **II**, cytotoxicity against human ovarian adenocarcinoma cells *SCOV3* and normal human fibroblast cells of the *HDF* line was determined. Based on the MTT test results, inhibition dose IC50 was calculated for each substance. Drugs that cause the death of tumor cells at minimum concentrations without disrupting the viability of normal cells are considered to be promising drugs. Complex **I** leads to the death of normal cells rather than tumor cells (Fig. 6). The IC50 values for *SCOV3* and *HDF* are

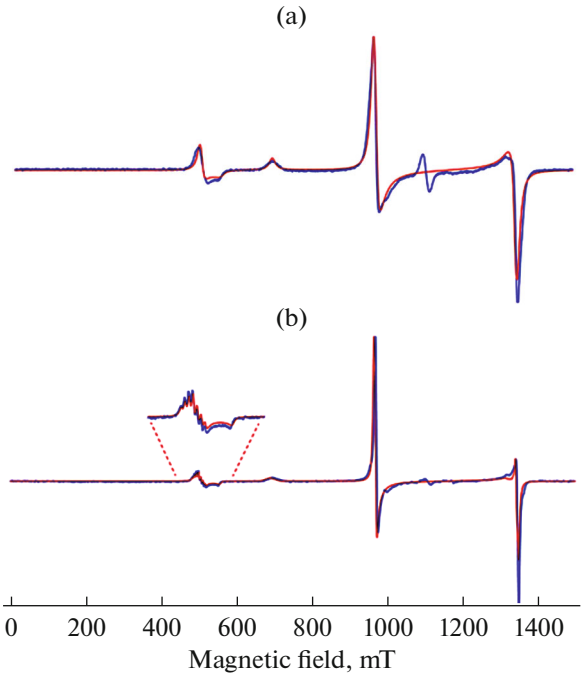

Fig. 5. EPR spectra of **I** in the Q-band region (33.8 GHz) at (a) 293 and (b) 150 K. Calculated spectra are shown in red (see parameters in the main text).

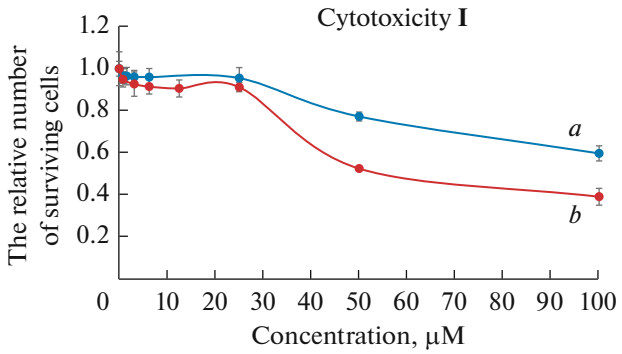

Fig. 6. Survival rates of the (*a*) *SCOV3* and (*b*) *HDF* cells incubated with various concentrations of complex **I** dissolved in DMSO. The mean value of the MTT index ± standard deviation calculated from three independent measurements is given.

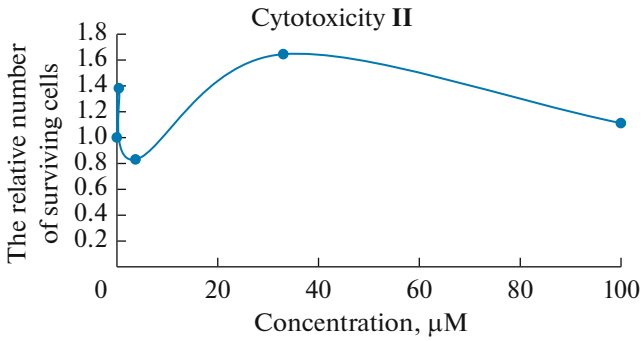

Fig. 7. Survival rates of the *SCOV3* cells incubated with various concentrations of complex **II** or DMSO as a control sample. The mean value of the MTT index ± standard deviation calculated from three independent measurements is shown.

>100 and 55 μmol/L, respectively. As expected, compound **II** has the opposite effect. It turned out that this complex stimulates the proliferation of tumor cells (Fig. 7). Thus, complex **II** also cannot be considered as a promising antitumor agent.

ACKNOWLEDGMENTS

The X-ray diffraction experiments were carried out with the support from the Ministry of Science and Higher Education of the Russian Federation using the scientific equipment of Center for Molecular Structure Study at the Institute of Organoelement Compounds, Russian Academy of Sciences. Elemental analyses and IR spectroscopy studies were performed using the equipment of Center for Collective Use of Physical Methods of Research at the Institute of General and Inorganic Chemistry, Russian Academy of Sciences.

FUNDING

This work was supported by the Russian Science Foundation (grant no. 20-13-00061).

Table 4. Results of the in vitro antibacterial activity of complexes **I** and **II** against *Mycolicibacterium smegmatis*

Compound	MIC, μg/disc	Inhibition zone, mm		Reference
	24 h	24 h	120 h	
I	122			This study
II	624	0*	0*	This study
$[Cu(Fur)_2(Phen)]$	2	7 ± 0.5**	7 ± 0.5**	[29]
$[Fe_3O(Fur)_6(THF)_3]\cdot 3THF$	13	7**	0*	[32]
$[Zn_2(Fur)_4Phpy_2]$	41	6.5 ± 0.5**	6.5 ± 0.5**	[29]
$[Zn(Fur)_2(Bipy)]$	44	6.5 ± 0.5**	6.5 ± 0.5**	[31]
$[Cu(Fur)_2(Bipy)(H_2O)]$	46	7 ± 0.5	7 ± 0.5***	[31]
$[Co_3(Fur)_6(Phen)_2]$	60	7 ± 0.5	7 ± 0.5***	[32]
$[Co_3O(Fur)_6(H_2O)_3]$	120	6.5 ± 0.3**	6.5 ± 0.3**	[32]
$[Co_6(Piv)_8(HPiv)_4(Fur)_2(OH)_2]$	143	6.5 ± 0.3**	0*	[32]
$[Cu_2(Fur)_4(Py)_2]$	146	7 ± 0.5	7 ± 0.5***	[29]
$[Cu(Fur)_2(Py)_2(H_2O)]$	153	7 ± 0.5	7 ± 0.5***	[29]
$[Cu(Fur)_2(Phpy)_2(H_2O)]\cdot Phpy$	224	7.0 ± 0.5	7.0 ± 0.5***	[34]
$[Ni(Fur)_2(Phen)(H_2O)_2]\cdot H_2O$	249	6.7 ± 0.3	6.7 ± 0.3***	[33]
$[Zn_2(Fur)_4Py_2]$	366	6.5 ± 0.3**	6.5 ± 0.3**	[29]
$[Ni(Fur)_2(Pz)_4]\cdot 2MeCN$	635	6.5 ± 0.5	0*	[33]
INH	100	7**	6.5**	
Rif	10	6.5	6.5***	
HFur	112	0*	0*	
Phen	9	0*	0*	
Bipy	78	0*	0*	

* 0, no inhibition zone.
** The growth inhibition zone of the bacterial culture, which is initially appeared after several hours of growth, starts to cover the entire zone surface.
*** The growth inhibition zone of the bacterial culture is not covered for the indicated time period.

CONFLICT OF INTEREST

The authors declare that they have no conflicts of interest.

REFERENCES

1. Koshechkin, V.A. and Ivanova, Z.A., *Tuberkulez* (Tuberculosis), Moscow: GEOTAR-Media, 2007.
2. Komissarova, O.G. and Abdullaev, R.Yu., *Mekhanizmy deistviya protivotuberkuleznykh preparatov* (Mechanisms of Action of Antituberculosis Drugs), Moscow: U Nikitskikh Vorot, 2014.
3. Bhat, Z.S., Rather, M.A., Maqbool, M., et al., *Biomed. Pharmacother.*, 2017, vol. 95, p. 1520.
4. Brill, A.S., *J. Biochem. Mol. Biol. Biophys.*, 1977, vol. 26, p. 1.
5. Punt, P.M. and Clever, G.H., *Chemistry*, 2019, vol. 25, p. 13987.
6. Drennan, C.L. and Peters, J.W., *Curr. Opin. Struct. Biol.*, 2003, vol. 13, p. 220.
7. Coelho, T.S., Halicki, P.C.B., Silva de Menezes, L., et al., *Lett. Appl. Microbiol.*, 2020, vol. 71, p. 146.
8. Chim, N., Johnson, P.M., and Goulding, C.W., *J. Inorg. Biochem.*, 2014, vol. 133, p. 118.
9. Krasnovskaya, O., Naumov, A., Guk, D., et al., *Int. J. Mol. Sci.*, 2020, vol. 21, p. 3695.
10. Rada, J.P., Bastos, B.S.M., Anselmino, L., et al., *Inorg. Chem.*, 2019, vol. 58, p. 8800.
11. Djoko, K.Y., Ong, C.L., Walker, M.J., and McEwan, A.G., *J. Biol. Chem.*, 2015, vol. 290, p. 18954.
12. Ovchinnikov, Yu.A., *Bioorganicheskaya khimiya* (Bioorganic Chemistry), Moscow: Prosveshchenie, 1987.
13. Ngwane, A.H., Petersen, R.D., Baker, B., et al., *IUBMB Life*, 2019, vol. 71, p. 532.
14. Tkachuk, V.A., *Klinicheskaya biokhimiya* (Clinical Biochemistry), Moscow: GEOTAR-Media, 2008.
15. Bol'shakov, A.M. and Novikov, I.M., *Obshchaya gigiena* (General Hygiene), Moscow: Meditsina, 2002.
16. Dimé, K.D.A., Cattey, H., Lucas, D., and Devillers, Ch.H., *Eur. J. Inorg. Chem.*, 2018, p. 4834.

17. Bhattacharjee, J., Harinath, A., Sarkar, A., and Panda, T.K., *ChemCatChem*, 2019, vol. 11, p. 1.
18. Nandi, S., Luna, Ph., Maity, R., Chakraborty, D., et al., *Mater. Horiz.*, 2019, vol. 6, p. 1883.
19. Paluchowska, B., Maurin, J.K., and Leciejewicz, J., *J. Chem. Cryst.*, 1997, vol. 27, p. 177.
20. Yang, J., Yin, X., Wu, L., et al., *Inorg. Chem.*, 2019, vol. 57, p. 150105.
21. Wan, K., Yu, J., Yang, Q., et al., *Eur. J. Inorg. Chem.*, 2019, p. 3094.
22. Roueindeji, H., Ratsifitahina, A., Roisnel, T., et al., *Chem.-Eur. J.*, 2019, vol. 26, p. 3535.
23. Anker, M.D., Kefalidis, C.E., Fang, Y.Y.J., et al., *J. Am. Chem. Soc.*, 2017, vol. 139, p. 10036.
24. Yuan, N., Zhang, M., Cai, H., et al., *Inorg. Chem. Commun.*, 2019, vol. 101, p. 130.
25. Li, N., Zhao, Z., Yu, C., et al., *Dalton Trans*, 2019, vol. 48, p. 9067.
26. Cole, L.B. and Holt, E.M., *Inorg. Chim. Acta*, 1989, vol. 160, p. 195.
27. *International Union of Crystallography. Tables for X-ray Crystallography*, Dodrecht: Kluwer Academic, 1995, p. 681.
28. Lenstra, A.T.H., *Bull. Soc. Chim. Belg.*, 1985, vol. 94, p. 161.
29. Lutsenko, I.A., Baravikov, D.E., Kiskin, M.A., et al., R*uss. J. Coord. Chem.*, 2020, vol. 46, no. 6, p. 411. https://doi.org/10.1134/S1070328420060056
30. Yambulatov, D.S., Nikolaevskii, S.A., Lutsenko, I.A., et al., *Russ. J. Coord. Chem.*, 2020, vol. 46, no. 11, p. 772. https://doi.org/10.1134/S1070328420110093
31. Lutsenko, I.A., Yambulatov, D.S., Kiskin, M.A., et al., *Russ. J. Coord. Chem.*, 2020, vol. 46, no. 12, p. 787. https://doi.org/10.1134/S1070328420120040
32. Lutsenko, I.A., Yambulatov, D.S., Kiskin, M.A., et al., *Chem. Select.*, 2020, vol. 5, p. 11837.
33. Uvarova, M.A., Lutsenko, I.A., Kiskin, M.A., et al., *Polyhedron*, 2021, vol. 203, p. 115241.
34. Lutsenko, I.A., Kiskin, M.A., Koshenskova, K.A., et al., *Russ. Chem. Bull.*, 2021, vol. 70, no. 3, p. 463.
35. Stoll, S. and Schweiger, A., *J. Magn. Reson.*, 2006, vol. 178, no. 1, p. 42.
36. Sheldrick, G.M., *Acta Crystallogr., Sect. A: Found. Adv.*, 2015, vol. 71, p. 3.
37. Dolomanov, O.V., Bourhis, L.J., Gildea, R.J., et al., *J. Appl. Crystallogr.*, 2009, vol. 42, p. 339.
38. Fedin, M.V., Bogomyakov, A.S., Romanenko, G.V., et al., *Dalton Trans.*, 2013, vol. 42, p. 4513.
39. Bondarenko, M.A., Novikov, A.S., Korolkov, I.V., et al., *Inorg. Chim. Acta*, 2021, vol. 524, p. 120436.
40. Paluchowska, B., Maurin, J.K., and Leciejewicz, J., *J. Chem. Cryst.*, 1997, vol. 27, p. 177.
41. Calvo, R., Abud, J.E., Sartoris, R.P., et al., *Phys. Rev.*, 2011, vol. 84, p. 104433.

Translated by O. Kadkin